Earthq Eng & Eng Vib (2021) 20: 303-316 **DOI**: https://doi.org/10.1007/s11803-021-2021-z

Seismic resilience assessment of corroded reinforced concrete structures designed to the Chinese codes

Yu Xiaohui[1†], Dai Kuangyu[1‡], Li Yushi[1§] and Li Bing[2†]

1. *School of Civil Engineering, Harbin Institute of Technology, Harbin 150090, China*

2. *School of Civil and Environmental Engineering, Nanyang Technological University, Singapore 639798, Singapore*

Abstract: The natural landscape in China exposes many existing RC buildings to aggressive environments. Such exposure can lead to deterioration in structural performance with regard to resisting events such as earthquakes. Corrosion of embedded reinforcement is one of the most common mechanisms by which such structural degradation occurs. There has been increasing attention in recent years toward seismic resilience in communities and their constituent construction; however, to date, studies have neglected the effect of natural aging. This study aims to examine the effect of reinforcement corrosion on the seismic resilience of RC frames that are designed according to Chinese seismic design codes. A total of twenty RC frames are used to represent design and construction that is typical of coastal China, with consideration given to various seismic fortification levels and elevation arrangements. Seismic fragility relationships are developed for case frames under varying levels of reinforcement corrosion, i.e., corrosion rates are increased from 5% to 15%. Subsequently, the seismic resilience levels of uncorroded and corroded RC frames are compared using a normalized loss factor. It was found that the loss of resilience of the corroded frames is greater than that of their uncorroded counterparts. At the Rare Earthquake hazard level, the corrosion-induced increase in loss of resilience can be more than 200%, showing the significant effect of reinforcement corrosion on structural resilience under the influence of earthquakes.

Keywords: seismic resilience; seismic fragility; corrosion; Chinese seismic design codes; RC frames

1 Introduction

Many parts of China are exposed to weather elements that would constitute an aggressive environment. This offers durability problems due to the degradation of material performance. Such an aggressive environment can cause significant corrosion in reinforcement (Enright and Frangopol, 1998), leading to the deterioration of the mechanical properties of reinforcing bars (Du *et al*., 2005), the cracking of cover concrete (Zhao *et al*., 2015), and a reduction in bar-concrete bond strength (Lundgren, 2007; Bhargava *et al*., 2007). These deterioration mechanisms that are caused by corrosion could significantly affect structural resistance against earthquakes (Yalciner *et al*., 2015; Liu *et al*., 2017; Dai *et al*., 2020a). Therefore, it is necessary to investigate the seismic performance of aging RC structures that exhibit corroded reinforcement.

In recent years, the concept of seismic resilience has attracted worldwide attention. Bruneau *et al*. (2003) proposed a conceptual framework for quantifying the seismic resilience of communities, which includes four dimensions: robustness, redundancy, resourcefulness and rapidity. This conceptual framework was extended by Cimellaro *et al*. (2010) to define the resilience of disasters. Moreover, Miles and Chang (2006) developed a conceptual model of community recovery by using Markov chains to simulate the recovery trajectory. All previous studies focused on seismic resilience from a regional-scale viewpoint. These studies demonstrated the consequences for and the recovery of the concerned region due to the effects of earthquakes. Unlike regional seismic resilience, numerous studies have also been conducted to improve structure-specific resilience with respect to earthquakes. For example, new types of building systems (Deierlein *et al*., 2011; Sabbagh *et al*., 2012) or structural elements (Wilkinson *et al*., 2006; Liu and Jiang, 2017) have been proposed. From a structure-specific resilience perspective, the enhancement of structural resilience is equal to the reduction of structural damage caused by earthquakes.

Through an overview of available studies, it is found that regional resilience and structure-specific

Correspondence to: Li bing, Civil and Environmental Engineering at Nanyang Technological University, Singapore 639798
Tel:
E-mail: cbli@ntu.edu.sg
[†]Associate Professor; [‡]PhD Candidate; [§]Master

Supported by: National Natural Science Foundation of China under Grant No. 51778198, and the Natural Science Foundation for Excellent Young Scientists of Heilongjiang Province under Grant No.YQ2020E023

Received November 19, 2020; **Accepted** February 8, 2021

resilience are not quantified in a consistent way. This is inconvenient for the extension of the resilience of individual structures in the context of a community. The regional resilience result also cannot be directly used to guild the design or retrofitting of individual structures. As noted by Cimellaro *et al*. (2010), the seismic resilience of individual structures should incorporate the interaction between the individual structures and the community. Based on this idea, it is important to evaluate structure-specific resilience as compatible with the strategy that was used in the regional resilience assessment (Wen *et al*., 2019). In recent years, several studies have focused on structural resilience by considering the effect of reinforcement corrosion. For example, Biondini *et al*. (2015) proposed a probabilistic lifetime assessment approach for quantifying the seismic resilience of concrete structures by considering corrosion-induced deterioration. This approach was then applied to a three-story concrete frame building and a four-span continuous concrete bridge. This approach showed the combined effects of corrosion and earthquakes on the time-varying performance of the system. Motlagh *et al*. (2020) evaluated seismic resilience for existing and corroded buildings by considering near-fault pulse-type ground motion. China has a long coastline with numerous RC structures located in a chloride environment. Therefore, the problem of reinforcement corrosion is severe in existing RC structures, which could cause a significant deterioration in the structural capacity to resist earthquakes. However, the seismic resilience of the corroded RC structures in China is not well documented.

To bridge this knowledge gap, this study aims to conduct a comprehensive investigation of the seismic resilience of aging RC frames that have been designed according to Chinese seismic design codes (GB50011-2010, 2010). To do this, a total of twenty RC frames have been designed with varying earthquake fortification levels and structural heights. The designed RC frames are used to represent typical designs and constructions of the RC frame in coastal areas of China. Fragility relationships are developed for case frames that are uncorroded and have experienced growing corrosion rates of 5%, 10%, and 15%. Subsequently, a normalized loss factor of resilience proposed by Wen *et al*. (2019) is used to quantify the resilience for uncorroded and corroded RC frames. Through comparisons, the effect of reinforcement corrosion on structural resilience is extracted.

2 Structural design and modeling

2.1 Structural design

The RC frames were designed by assuming they are located in the eastern coastal regions of China. Sixty-six cities in the target regions were considered. Design requirements corresponding to the cities in the study were collected from GB50010-2010 (2010) and GB50011-2010 (2010) with regard to seismic fortification levels, wind loads, and snow loads. To make the structural designs representative, the method used in the global earthquake model (GEM) (D'Ayala D *et al*., 2014) was adopted to determine design variables, with high, medium and low levels. In this study, four important design variables were considered, which included the number of stories, bay width, the axial loading ratio of columns, and the period reduction factor, taking into account the contribution of infill walls to structural stiffness. Therefore, a total of four groups of RC frames were designed with varying story numbers, bay widths, axial force ratios, and period reduction factors. In the building group with varying story numbers, six and nine stories were chosen to represent the low-to-medium height of RC frames. Three types of bay widths, 6.0 m, 7.2 m, and 8.4 m, were considered. Two commonly used axial force ratios, 0.65 and 0.73, were selected as the basic ratios for nine- and six-story RC frames. For the high and low level of axial force ratio, the basic ratios should be increased or decreased by 0.1, respectively. As for the period reduction factors, they were considered to be varied as 0.85 and 0.7, corresponding to the low and high contributions of infill walls to the structural stiffness. Table 1 summarizes the designed frames and the corresponding design variables. Figure 1 shows the plan and elevation views of the designed frames. All the frames were designed with the same plan arrangement. The reinforcement details and the geometric sizes of columns and beams are provided in Fig. 2 and Table 2.

2.2 Structural modeling and validation

OpenSees was used to develop analytical models and simulate the inelastic behavior of structures experiencing the effects of an earthquake (Mckenna, 2011; Yu *et al*., 2018). A two-dimensional model was used for the case RC frames owing to the limited torsional effects. Beams and columns were modeled using nonlinear force-based beam-column elements, with plasticity concentrating over a specified hinge length at element ends (Scott and Fenves, 2006). In the plastic concentrating regions, the fiber-type sections were used and discretized into fibers as reinforcement bars and confined (core) and unconfined (cover) concrete. The fiber section did not consider the shear-critical failure model of RC elements (Ning *et al*., 2019). For unconfined concrete, its inelastic behavior was represented by a nonlinear constitutive model with degraded linear unloading/reloading stiffness, and tensile strength is not given (Kent and Park, 1971). Regarding confined concrete, the model proposed by Mander *et al*. (1988) was used to account for the confinement effect offered by the stirrup. The reinforcement bars were represented by a uniaxial tri-linear hysteretic material model with a pinching effect and degradation of stiffness and strength due to damage. Aside from the above, a zero-length element was defined at the ends of columns and

Table 1 Structural designs and the varying design variables

Building group	Number	Story number	Bay width	Axial force ratio	Period reduction factor
Varying of story number	S61	6	7.2	0.79	0.70
	S62	6	7.2	0.73	0.70
	S63	6	7.2	0.73	0.70
	S64	6	7.2	0.64	0.70
	S65	6	7.2	0.41	0.85
	S91	9	7.2	0.75	0.70
	S92	9	7.2	0.65	0.70
	S93	9	7.2	0.65	0.70
	S94	9	7.2	0.59	0.70
	S95	9	7.2	0.47	0.85
Varying of bay width	SA62	6	8.4	0.76	0.70
	SA92	9	8.4	0.64	0.70
	SR62	6	6.0	0.71	0.70
	SR92	9	6.0	0.62	0.70
Varying of axial force ratio	SW62	6	7.2	0.84	0.70
	SW92	9	7.2	0.75	0.70
	SS62	6	7.2	0.63	0.70
	SS92	9	7.2	0.56	0.70
Varying of the period reduction factor	SP65	6	7.2	0.37	0.70
	SP95	9	7.2	0.50	0.70

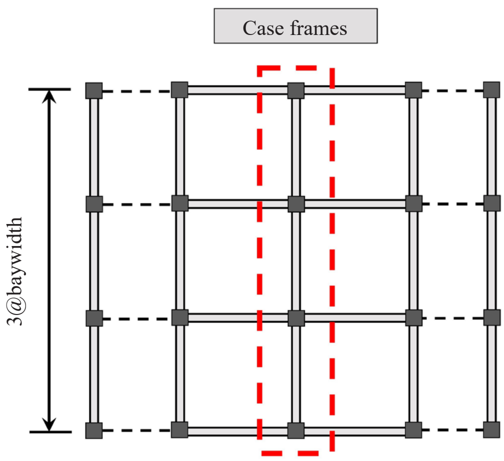

(a) Plan view

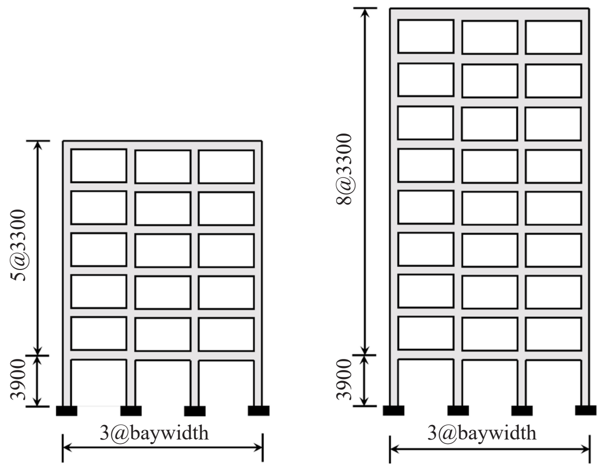

(b) Elevation view

Fig. 1 Plan and elevation views of case RC frames (unit: mm)

beams between two nodes at the same location. A single fiber section was used to represent the force-deformation relationship for the zero-length element. Unlike the fiber section outside the zero-length element, the fiber section in the zero-length element adopted a uniaxial material model for reinforcement bars by considering bond-slip due to strain penetration (Zhao and Sritharan, 2007). Figure 3 summarizes the overall structural modeling details.

Due to the limitation of experimental conditions,

Table 2 Geometry sizes and reinforcement details of the case RC frames

Frames	Story number	Bay width	Columns					Beams				
			Geometry size	Longitudinal reinforcement			Transverse reinforcement	Geometry size	Longitudinal reinforcement			Transverse reinforcement
				Part A	Part B	Part C			Part D	Part E	Part F	
S61	6	7.2	600×600	4×18	4×18	4×18	8@100/200	300×600	4×25	4×22	4×12	8@100/200
S62	6	7.2	600×650	4×18	4×18	6×18	8@100/200	300×600	4×25	4×22	4×12	8@100/200
S63	6	7.2	600×650	5×18	5×18	6×18	8@100/200	300×600	2×25+2×22 /2×22	4×22	4×12	8@100/200
S64	6	7.2	600×650	6×25	6×25	8×25	8@100	300×700	4×22/ 4×22	2×25+ 2×22	4×12	8@100/150
S65	6	7.2	Story 1-2: 750×750 Story 3-6: 700×700	9×25	9×25	14×25	8@100/150	400×700	6×22/ 5×22	4×25+ 1×22	4×12	8@100/200
S91	9	7.2	650×650	5×18	5×18	6×18	10@100/200	300×600	4×22/ 2×22	3×25	4×12	8@100/200
S92	9	7.2	Story 1: 700×700 Story 2-9: 650×650	6×18	6×18	8×18	10@100/150	300×600	4×22/ 2×22	3×25	4×12	8@100/200
S93	9	7.2	Story 1: 700×700 Story 2-9: 650×650	7×18	7×18	8×18	10@100/150	300×600	4×22/ 4×22	4×22	4×12	8@100/150
S94	9	7.2	Story 1: 700×700 Story 2-9: 650×650	8×25	8×25	10×25	10@100/200	400×700	6×22/ 3×22	5×22	4×12	10@100/200
S95	9	7.2	Story 1-3: 850×850 Story 4-6: 750×750 Story 7-9: 650×650	11×25	11×25	16×25	10@100/200	400×750	6×22/ 5×22	2×25+ 4×22	4×14	10@100/200
SA62	6	8.4	650×650	5×18	5×18	6×18	8@100/200	300×700	4×22/ 4×22	2×22/ 5×22	4×12	8@100/150
SA92	9	8.4	Story 1-2: 800×800 Story 3-9: 700×700	7×18	7×18	10×18	10@100	300×700	4×25/ 2×22	4×25	4×12	8@100/200
SR62	6	6	500×550	4×18	4×18	4×18	8@100/200	300×500	4×22	3×22	4×12	8@100/200
SR92	9	6	600×600	5×18	5×18	6×18	10@100/150	300×500	4×25	3×22	4×12	8@100/200
SW62	6	7.2	500×500	4×18	4×18	4×18	8@100/200	300×600	2×22+2×25	3×25	4×12	8@100/200
SW92	9	7.2	650×650	5×18	5×18	6×18	10@100/150	300×600	4×22/ 2×22	3×25	4×12	8@100/200
SS62	6	7.2	600×650	4×18	4×18	4×18	8@100/200	300×600	4×25	4×22	4×12	8@100/200
SS92	9	7.2	Story 1: 700×700 Story 2-9: 650×650	6×18	6×18	8×18	10@100/150	300×600	4×22/ 2×22	3×25	4×12	8@100/200
SP65	6	7.2	Story 1-2: 750×750 Story 3-6: 700×700	10×25/ 4×25	10×25/ 4×25	16×25	10@100	400×800	6×22/ 6×22	5×25+ 2×22	6×12	8@100/200
SP95	9	7.2	Story 1-3: 850×850 Story 4-6: 750×750 Story 7-9: 650×650	11×25+ 5×25	20×25	11×25+ 5×25	10@100	400×800	6×22/ 6×22	4×25+ 3×22	6×12	10@100/200

Note: Longitudinal reinforcement is represented by the number of reinforcing bars times the corresponding diameter (mm). For example, 4×18 means 4 bars with a diameter of 18 mm. Two layers of longitudinal reinforcing bars are represented by the first reinforcement layer/the second reinforcement layer. For example, 4×22/2×22 means the first reinforcement layer has 4 bars with a diameter of 22 mm, and the second reinforcement layer has 2 bars with a diameter of 22 mm. The transverse reinforcement is arranged in a smaller spacing at the plastic hinge areas of columns and beams, while it is arranged with a larger spacing outside the plastic hinge areas.

experimental studies have rarely been conducted to investigate the seismic performance of corroded RC frames. Therefore, the modeling strategy used in this study is validated through simulating the hysteretic behaviors of two corroded column specimens that were tested by Dai *et al*. (2020b). The details of the tests are not provided herein but may be referred to elsewhere (Dai *et al*., 2020b). The two test specimens are designed with the same geometric size and reinforcement details. They are labeled C-E5-0.1, and C-E10-0.1 (Dai *et al*., 2020b), corresponding to the low to medium corrosion rates of reinforcement of 5% and 10%, respectively. Figure 4 compares the simulated and experimental data for the three specimens. It is clear that the adopted structural modeling strategy effectively simulates the test data of uncorroded and corroded columns, showing the reliability of the adopted structural model. A reliable structural model is beneficial for the following assessment of seismic resilience for corroded RC frames.

2.3 Modelling consideration for reinforcement corrosion

In this study, reinforcement corrosion caused by the penetration of chloride ions was considered, which can lead to four types of deterioration mechanisms, including 1) the loss of a longitudinal reinforcement section, 2) the reduction of reinforcement strength and ductility, 3) the degradation of compressive strength of concrete cover, and 4) the deterioration of bond-slip performance. Table 3 summarizes the mathematical models adopted to represent the above-stated deterioration mechanisms due to reinforcement corrosion. The mathematical modeling details of the first three deterioration mechanisms can be found in Yu *et al.* (2017a). With regard to bond-slip deterioration, a reduction ratio R_c of the bond strength $\tau_{c,corr}$ at any corrosion level to the original bond strength $\tau_{c,0}$ is used herein according to Chung *et al*. (2004), which is expressed by

$$R_c = \frac{\tau_{c,corr}}{\tau_{c,0}} \tag{1}$$

In this study, the empirical equations proposed by Xu (2003) are used to relate R_c to the corrosion rate η_s, as

$$R_c = 1 + 0.5625\eta_s - 0.3375\eta_s^2 + 0.055625\eta_s^3 - 0.003\eta_s^4 \quad \text{for} \quad 0 < \eta_s < 7\% \tag{2}$$

$$R_c = 2.0786\eta_s^{-1.0369} \quad \text{for} \quad 7\% < \eta_s \tag{3}$$

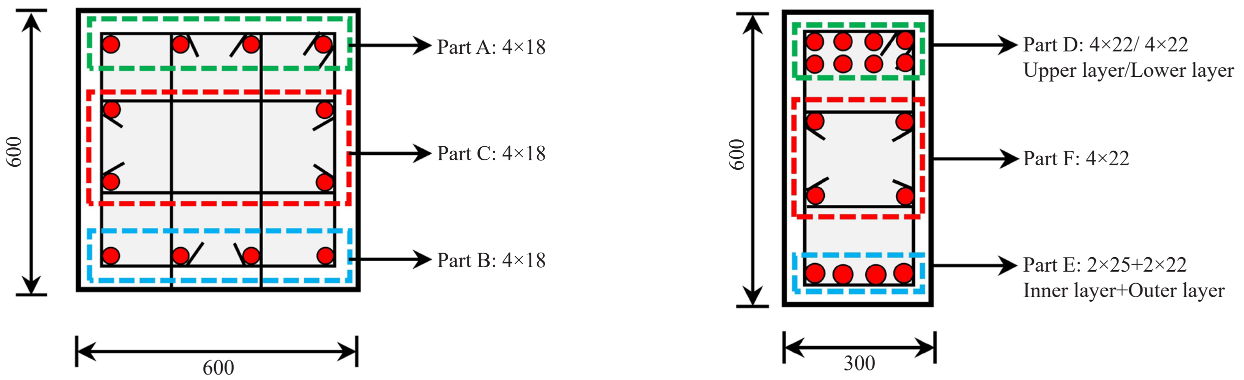

Fig. 2 Typical reinforcement details of the columns and beams

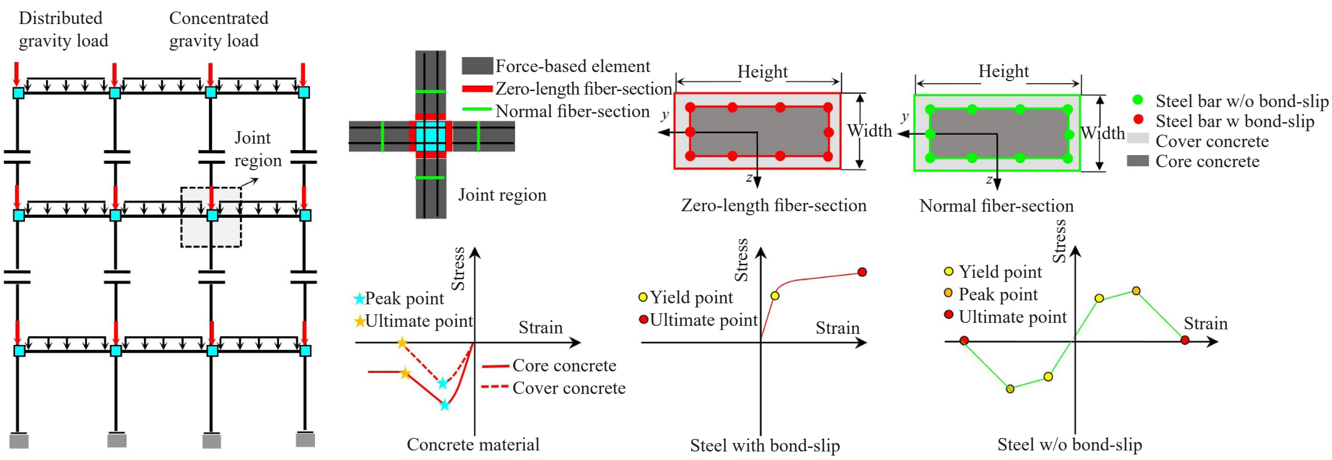

Fig. 3 Illustration of the structural modeling strategy

3 Seismic fragility assessment of RC frames under corrosion

3.1 Seismic fragility function

Seismic fragility is described by the probability of structural demand reaching or exceeding stipulated limit states (LSs) as a function of a ground motion intensity measure. The seismic fragility function is termed $f_{LS}\left(S_a = x\right)$, where spectral acceleration, S_a, in the fundamental period of a structure with a 5% damping ratio was adopted to represent the intensity of ground motion acceleration. A widely accepted lognormal distribution function was adopted herein for fragility assessment (Wen *et al*., 2004), which is expressed by

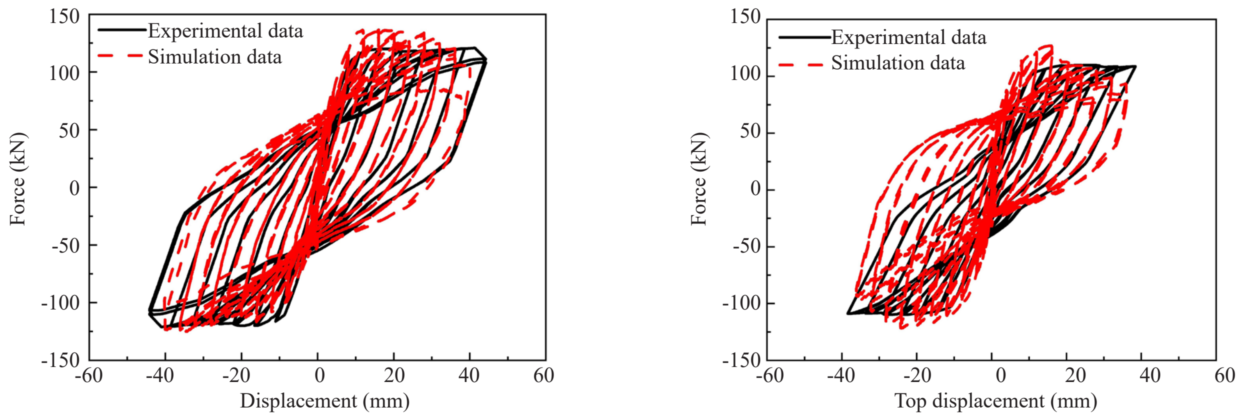

(a) Specimen C-E5-0.1 (b) Specimen C-E10-0.1

Fig. 4 Simulated and tested hysteretic curves for Specimens C-E5-0.1 and C-E10-0.1 in Dai *et al.* (2020b)

Table 3 Mathematical models adopted to represent deterioration mechanisms due to corrosion

Deterioration mechanisms	Numerical models	Important parameters	Reference
Loss of longitudinal reinforcement section	$A'_{\mathrm{s}} = \dfrac{\pi D^2}{4}(1-\eta_{\mathrm{s}})$	A'_{s}: cross-section area of the corroded reinforcing bars; D: diameter of the uncorroded reinforcement.	Ghosh and Padgett (2010)
Reduction of reinforcement strength	$f'_{\mathrm{y}} = (1-0.5\times\eta_{\mathrm{s}})\times f_{\mathrm{y}}$ $f'_{\mathrm{u}} = (1-0.5\times\eta_{\mathrm{s}})\times f_{\mathrm{u}}$	f'_{y} and f_{y}: yield strengths of the corroded and uncorroded reinforcing bars, respectively; f'_{u} and f_{u}: ultimate strength of the corroded and uncorroded reinforcing bars, respectively.	Du (2005)
Reduction of reinforcement ductility	$\varepsilon'_{\mathrm{u}} = (1-3\times\eta_{\mathrm{s}})\times\varepsilon_{\mathrm{u}}$	$\varepsilon'_{\mathrm{u}}$ and ε_{u}: ultimate elongation of the corroded and uncorroded reinforcing bars, respectively.	Cairns (2005)
Degradation of compressive strength of concrete cover	$f'_{\mathrm{c}} = \dfrac{f_{\mathrm{c}}}{1+K\varepsilon_1/\varepsilon_{\mathrm{c0}}}$ $\varepsilon_1 = (b_{\mathrm{f}}-b_0)/b_0$ $b_{\mathrm{f}}-b_0 = n_{\mathrm{c}}\times\omega_{\mathrm{cr}}$ $\omega_{\mathrm{cr}} = 2\pi(v_{\mathrm{rs}}-1)X$	f'_{c} and f_{c}: compressive strengths of concreter cover after and before cracking led by reinforcement corrosion; K: coefficient related to reinforcement roughness and diameter, where K = 0.1 is taken herein for medium-diameter ribbed reinforcement; $\varepsilon_{\mathrm{c0}}$: strain at the peak compressive stress of concrete cover; ε_1: average tensile strain of the cracked concrete; b_0 and b_{f}: cross-section widths of the concrete cover before and after cracking, respectively; n_{c}: number of reinforcements in the compression area; ω_{cr}: width of concrete cracking; v_{rs} is the volume expansion ratio of corrosion products; X: depth of the corrosion attack equal to the reduction of in reinforcement radius.	Coronelli and Gambarova (2004)
Reduction of bond-slip		Eqs. (1)–(3)	Chung *et al*. (2004); Xu (2003)

$$f_{LS}\left(S_a = x\right) = P\left(LS \mid S_a\right) = 1 - \Phi\left(\frac{\ln m_C - \ln m_{D|S_a}}{\sqrt{\beta_C^2 + \beta_{D|S_a}^2 + \beta_{\mathrm{M}}^2}}\right) = \Phi\left(\frac{\ln m_C - \ln m_{D|S_a}}{\sqrt{\beta_C^2 + \beta_{D|S_a}^2 + \beta_{\mathrm{M}}^2}}\right) \tag{4}$$

where $P\left(LS \mid S_a\right)$ denotes the exceeding probability of a predefined LS conditioned on $S_a = x$; $\Phi(\cdot)$ represents the standard normal probability integral; $m_{D|S_a}$ and $\beta_{D|S_a}$ are median and the standard deviation of the natural logarithm of the structural demand D on the condition of $S_a = x$, respectively; and m_C and β_C are median and the standard deviation of the natural logarithm of limit state capacity C, respectively; and β_{M} is used to denote uncertainty due to the imperfection of analytical modeling. The value of β_{M} is taken as 0.2 based on the assumption that the modeling process yields a response that is within ±30% of the actual value, with 90% confidence (Wen *et al.*, 2004).

For the seismic demand parameters, i.e., $m_{D|S_a}$ and $\beta_{D|S_a}$, they are quantified from the statistics of the inelastic structural response under earthquakes. The maximum drift ratio, $\theta_{\max}$, is taken herein as the engineering demand parameter to quantify D and C. A cloud method is used to generate a linear relationship between $\theta_{\max}$ and S_a at a log-log space, yielding (Shome *et al.*, 1998; Miano *et al.*, 2018)

$$\ln m_{D|S_a} = a + b\ln S_a \tag{5}$$

$$\beta_{D|S_a} = \sqrt{\frac{\sum_{i=1}^{N}\left(\ln D_i - \ln m_{D|S_a}\right)}{N-2}} \tag{6}$$

where a and b are coefficients determined by regression; N is the number of input ground motion records; and D_i is the drift response caused by the ith ground motion record.

Three limit states expressed as immediate occupancy (IO), life safety (LS), and collapse prevention (CP) are considered herein. Their median drift capacities m_C are defined as $\theta_{\max} = 1\%$, 2% and 4%, respectively (FEMA 273, 1997). Similar definitions have also been adopted in other studies (Ramamoorthy *et al.*, 2006; Ellingwood *et al.*, 2007; Howary and Mehanny, 2011) to quantify m_C. According to Wen *et al.* (2004), the variation in drift capacities is assumed to be $\beta_C = 0.3$ for all limit states, a figure also used in Ramamoorthy *et al.* (2006) and Hueste and Bai (2007).

Substituting Eq. (5) into Eq. (4), the five-parameter fragility function shown in Eq. (4) can be transformed into a function with only two parameters, yielding (Lu *et al.*, 2014; Yu *et al.*, 2017b)

$$f_{LS}\left(S_a = x\right) = \Phi\left[\frac{\ln m_{D|IM} - \ln m_C}{\sqrt{\beta_{D|IM}^2 + \beta_C^2 + \beta_{\mathrm{M}}^2}}\right] = \Phi\left[\frac{a + b\ln S_a - \ln m_C}{\sqrt{\beta_{D|IM}^2 + \beta_C^2 + \beta_{\mathrm{M}}^2}}\right] = \Phi\left[\frac{\ln\left(S_a / m_{\mathrm{R}}\right)}{\beta_{\mathrm{R}}}\right] \tag{7}$$

where m_{R} denotes the fragility median corresponding to a failure probability of 50%, and β_{R} denotes fragility dispersion, showing the total variation of fragility. The values of m_{R} and β_{R} can be calculated by the following equations, respectively, as

$$m_{\mathrm{R}} = \left[m_C / \exp(a)\right]^{1/b} \tag{8}$$

$$\beta_{\mathrm{R}} = \frac{1}{b}\sqrt{\beta_{D|IM}^2 + \beta_C^2 + \beta_{\mathrm{M}}^2} \tag{9}$$

Figure 5 shows the effect of m_{R} and β_{R} on the shape of a fragility curve. It was found that m_{R} dominates the global location of the fragility curve and its variation can lead to a global shift in the curve. The value of β_{R} controls the slope of the fragility curve. The fragility curve is growing steeply when β_{R} is decreased. The transformed fragility function in Eq. (7) was used to extract the effect of reinforcement corrosion in the following sections.

3.2 Ground motion records

A total of 100 ground motion records was selected from the PEER Ground Motion Database (Ancheta *et al.*, 2013). The detailed information in these ground motion records can be found in Lu *et al.* (2014) and Yu *et al.* (2017b). Figure 6 shows the distribution of the selected ground motions in the space of earthquake magnitude (M_{w}) and distance (R). It is clear that the selected ground motions cover a wide M_{w}–R range. In a region with a low

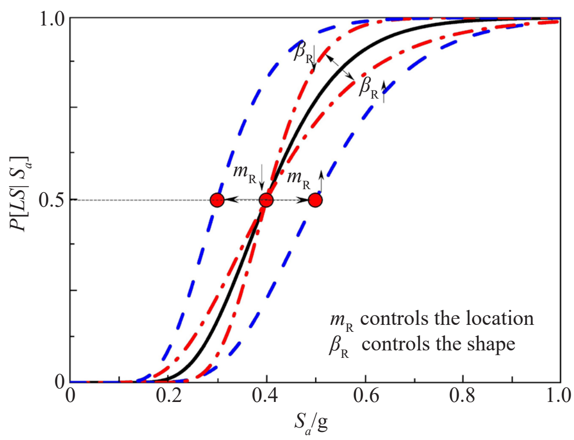

Fig. 5 Effect of m_{R} and β_{R} on a fragility curve

M_w and a small R, the largest number of ground motion records was selected since it is the most unfavorable measure among the four that were considered four M_w–R regions. As for the M_w–R region with a small M_w and a large R, the fewest ground motion records were selected due to their insignificant damage potential for structures. The directivity pulse-type effects of near-fault ground motions were not considered and the R values of the selected ground motion records are greater than 10 km. Besides, all the ground motions were recorded on NEHRP soil types C or D (stiff soil or soft rock) sites. These soil types are similar to the soil condition found at the target building site.

3.3 Fragility curves of corroded RC frames

Three corrosion rates of reinforcing bars, i.e., $\eta_s = 5\%, 10\%$ and 15%, were considered in correspondence to the low, medium, and high corrosion levels of structures, respectively. The intact frames without corroded reinforcement were also examined for comparison. A total of $4 \times 20 = 80$ frame cases were considered to develop their fragility curves. The numerical models for the corroded RC frames were developed according to Section 2.2 by considering deterioration mechanisms due to reinforcement corrosion (see Section 2.3). The uncorroded and corroded RC frames were subjected to 100 selected ground motion records. Through nonlinear time-history analyses, the structural responses in terms of θ_{max} were obtained. Next, the seismic demand model parameters, i.e., $m_{D|S_a}$ and $\beta_{D|S_a}$, were calculated through regressions between $\ln S_a$ and $\ln m_{D|S_a}$ (see Eq. (5) and Eq. (6)). The seismic demand parameters ($m_{D|S_a}$ and $\beta_{D|S_a}$) and the limit state capacity parameters (m_C and β_C) were substituted into Eq. (4). Finally, the seismic fragility curves of corroded and uncorroded RC frames were generated. At a given limit state, the fragility curves of the uncorroded and corroded structures were compared to investigate the effect of reinforcement corrosion on seismic performance.

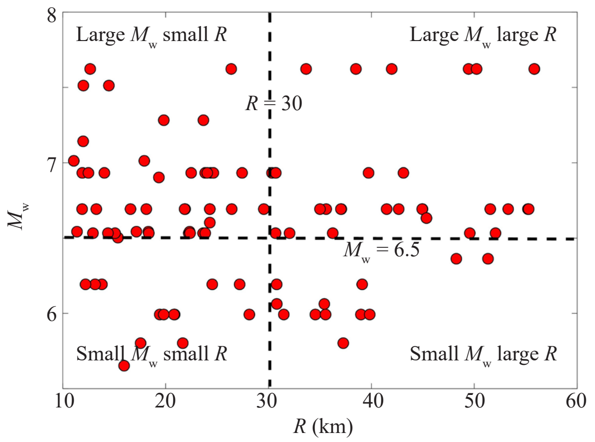

Fig. 6 Distribution of the selected ground motion records in M_w-R bins

The frame labeled S61 was taken alone as an example for illustration. Figure 7 shows the fragility curves of this structure, subjected to different levels of corrosion. It was observed that the difference of fragility curves corresponding to the cases with η_s = 10% and η_s = 15% are limited compared to those corresponding to the cases with η_s = 5% and η_s = 10%, as well as the cases with uncorroded reinforcement and η_s = 5%. In particular, at the IO limit state, the fragility curves of the corroded structures with η_s = 10% and η_s = 15% are almost identical to each other. Besides that, the fragility curves of the uncorroded structures are significantly different from those of the slightly corroded structure with η_s = 5%. This phenomenon was also observed in Afsar *et al*. (2018), which shows that the occurrence of reinforcement corrosion leads to a clear reduction of structural performance. Besides, at the CP limit state, there is an intersection between the fragility curve of the uncorroded structure and that of the corroded structure with η_s = 5% since reinforcement corrosion leads to a clear effect on fragility dispersion β_R (β_R controls the slope of the fragility curve, as shown in Fig. 5). It is noteworthy that the effect of the corrosion rate on fragility is complex since it is related to the numerical modeling approach of uncorroded and corroded structures, in addition to the adopted mathematical models of deterioration mechanisms due to reinforcement corrosion. Therefore, there is a considerable model error in the evaluation of fragility for corroded structures.

3.4 Effect of reinforcement corrosion on fragility parameters

The effect of reinforcement corrosion on the fragility median m_R and dispersion β_R is examined in this section. A ratio α_m between the fragility median for the corroded frame and that of the intact frame is defined, which is expressed by

$$\alpha_m = \frac{m_{R,\,corr}}{m_{R,\,int}} \tag{10}$$

where $m_{R,\,corr}$ and $m_{R,\,int}$ denote the fragility medians for the corroded and uncorroded frames, respectively.

Figure 8 shows the relationship between α_m and η_s, which was generated using the analysis data for the S61 frame at the IO limit state. An exponent-form function was used to represent the changing law of α_m on η_s, as

$$\alpha_m = A\mathrm{e}^{(-B\eta_s)} + (1 - A) \tag{11}$$

where A and B are the coefficients determined through regression.

Table 4 shows the obtained A and B values for different RC frame cases and the corresponding coefficient of determination R^2. It is clear that Eq. (10)

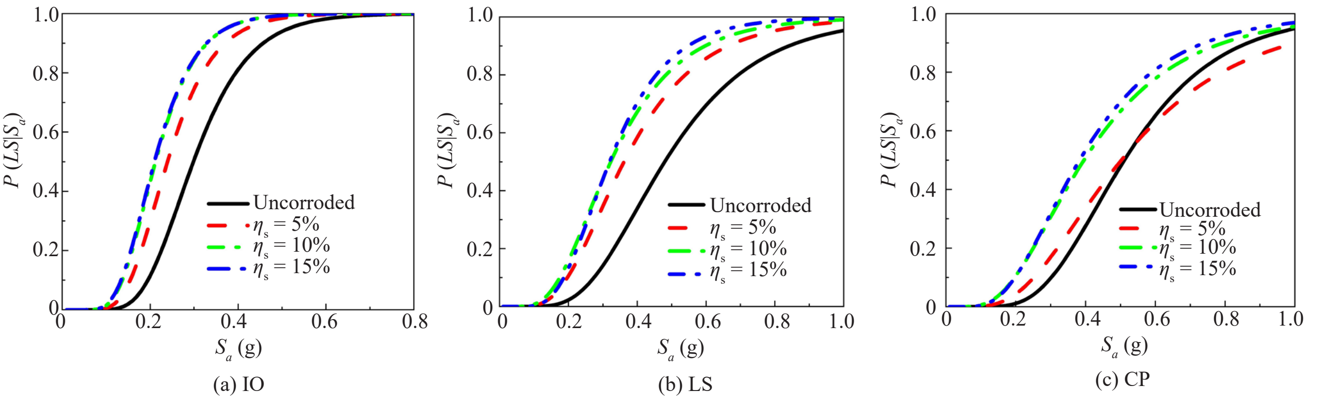

Fig. 7 Seismic fragility curves for the uncorroded and corroded RC frame S61

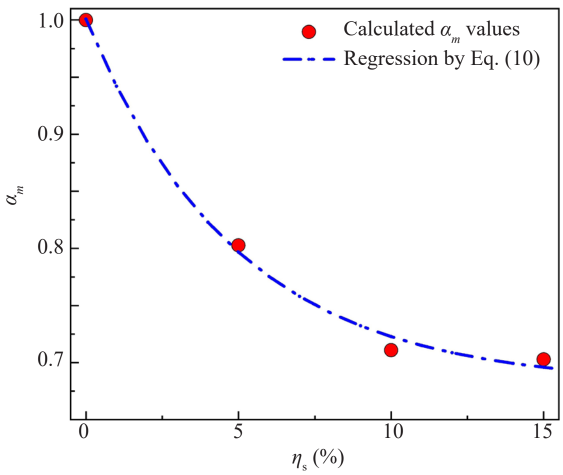

Fig. 8 Regressed relationship between α_m and η_s

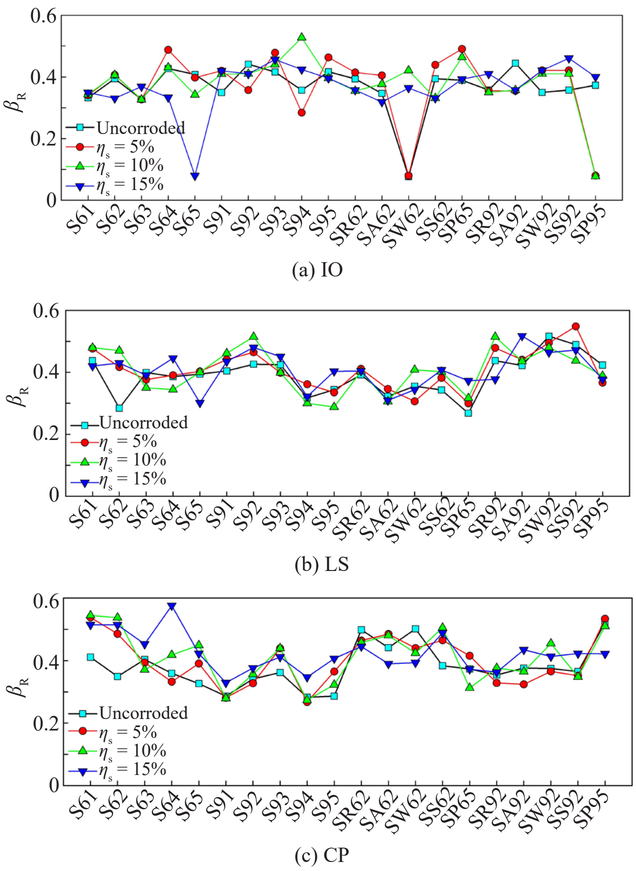

Fig. 9 β_R values for different case frames at the limit states of IO, LS, and CP

can well fit the relationship between α_m and η_s. To summarize the results in Table 4, the A and B values corresponding to different limit states are recommended to be in the scopes listed in Table 5. Figure 9 shows the obtained β_R values for different case frames at the limit states of IO, LS, and CP. Nevertheless, no clear trend was observed between β_R and η_s. Therefore, the median values of β_R corresponding to different limit states and different corrosion levels are calculated in Table 6.

4 Seismic resilience of corroded RC frames

4.1 The loss factor of resilience

The normalized loss factor of resilience, L_R, proposed by Wen *et al.* (2019) was adopted herein to measure the resilience of structures subjected to the effects of earthquakes, which is expressed by

$$R_{\mathrm{Loss}} = \frac{1}{\left[Q\left(t<t_0\right)\right]\cdot\left(t_1-t_0\right)}\int_{t_0}^{t_1}\left[Q\left(t<t_0\right)-Q\left(t\right)\right]\mathrm{d}t \tag{12}$$

where $Q(t)$ is the functionality of the structure, with its value varying from 0 to 1.0; t_0 is the time at which an earthquake occurs; and t_1 denotes the time at which structural functionality is recovered to target functionality Q_{target} at the end of the recovery process. It is noteworthy that Q_{target} should not be less than $Q(t<t_0)$ (i.e., $Q_{\mathrm{target}} \geq Q(t<t_0)$). Moreover, $Q(t<t_0)$ is less than 1.0 for aging structures due to functionality degradation. Figure 10 illustrates the concept of the loss factor of resilience defined by Eq. (11).

As noted by Cimellaro *et al.* (2010), $Q(t)$ is a function related to earthquake intensity, economic loss,

Table 4 Regressed coefficients *A* and *B* for different frames at IO, LS, and CP limit states

Frame	IO			LS			CP		
	A	*B*	R^2	*A*	*B*	R^2	*A*	*B*	R^2
S61	0.32	0.2	0.99	0.35	0.25	0.99	0.26	0.12	0.75
S62	0.30	0.25	0.98	0.3	0.12	0.95	0.19	0.20	0.99
S63	0.29	0.09	0.95	0.31	0.16	0.99	0.4	0.11	0.99
S64	0.25	0.08	0.95	0.5	0.05	0.99	0.36	0.09	0.99
S65	0.29	0.19	0.95	0.41	0.07	0.99	0.31	0.30	0.71
S91	0.20	0.08	0.98	0.24	0.13	0.97	0.19	0.09	0.83
S92	0.42	0.05	0.83	0.42	0.08	0.95	0.17	0.07	0.92
S93	0.38	0.24	0.99	0.34	0.15	0.96	0.25	0.07	0.95
S94	0.34	0.09	0.99	0.31	0.12	0.99	0.43	0.07	0.99
S95	0.32	0.15	0.99	0.34	0.15	0.98	0.38	0.10	0.94
SA62	0.40	0.2	0.99	0.26	0.10	0.85	1.67	0.01	0.99
SA92	0.34	0.04	0.99	0.28	0.10	0.88	0.32	0.04	0.91
SR62	0.35	0.05	0.98	0.21	0.23	0.99	0.16	0.21	0.98
SR92	0.41	0.06	0.95	0.36	0.11	0.99	0.41	0.03	0.98
SW62	1.36	0.03	0.93	0.35	0.04	0.97	0.24	0.06	0.97
SW92	0.27	0.11	0.99	0.22	0.19	1.00	0.66	0.02	0.95
SS62	0.32	0.25	0.97	0.38	0.07	0.95	0.39	0.07	0.89
SS92	0.28	0.21	0.99	0.26	0.29	0.96	0.67	0.02	0.88
SP65	0.83	0.03	0.97	0.48	0.09	0.98	0.55	0.17	0.99
SP95	0.39	0.09	0.96	0.48	0.19	0.99	0.53	0.24	0.95

Table 5 Ranges of the coefficients *A* and *B* at IO, LS, and CP limit states

Coefficients	IO	LS	CP
A	(0.25, 0.45)	(0.20, 0.50)	(0.15, 0.55)
B	(0.05, 0.25)	(0.05, 0.25)	(0.05, 0.25)

Table 6 Mean value of β_R for limit states of IO, LS, and CP

	IO	LS	CP
Uncorroded	0.38	0.39	0.37
$\eta_s = 5\%$	0.40	0.41	0.37
$\eta_s = 10\%$	0.40	0.40	0.38
$\eta_s = 15\%$	0.38	0.41	0.37

and recovery function, associated with recovery time and recovery path. In this study, functionality $Q(t)$ is defined by

$$Q(t) = Q(t < t_0) - L(S_a, T_r) \times \left[H(t - t_0) - H(t - t_1)\right] \times f_{\text{rec}}(t, t_0, T_r) \tag{13}$$

where T_r is the recovery time, determined by $t_1 - t_0$; $L(S_a, T_r)$ is the loss function; $H(t)$ is the Heaviside step function; $f_{\text{rec}}(t, t_0, T_r)$ is the recovery function.

There are commonly three types of recovery functions, including the linear, exponential function and trigonometric (Cimellaro *et al*., 2010). In this study, a linear functionality $Q(t)$ was adopted herein as a preliminary trial, which is expressed by

$$f_{\text{rec}}(t, T_r) = \left(1 - \frac{t - t_0}{T_r}\right) \tag{14}$$

4.2 Seismic loss estimation

The seismic loss of structures can be generally categorized into direct and indirect varieties. For the purpose of simplicity, only direct loss was considered herein. However, the current study can be extended by including indirect loss. The direct loss of the aging frames due to earthquakes is computed by

$$L = \sum_{i=1}^{4} R_{DS_i} \times P(DS_i \mid S_a) \tag{15}$$

where R_{DS_i} is the loss ratio of the damaged structure in the ith damage state, i.e., DS_i; $P(DS_i \mid S_a)$ is the failure probability of the structure at DS_i, which can be determined by the difference of failure probabilities of adjacent limit states, yielding

$$P\left(DS_i|S_a\right)=\begin{cases}P\left(LS_{i+1}|S_a\right)-P\left(LS_i|S_a\right) & i<4\\ P\left(LS_4|S_a\right) & i=4\end{cases} \tag{16}$$

where the failure probabilities of $P\left(LS_{i+1}|S_a\right)$ and $P(LS_i\,|\,S_a)$ are determined from the fragility curves listed in Section 3.

Three limit states in terms of IO, LS, and CP divide structural performance into four states of damage, i.e., $DS_i\left(i=1,2,3,4\right)$ The loss ratio R_{DS_i} is determined between the direct loss and the replacement cost. Table 7 provides the R_{DS_i} values corresponding to $DS_i\left(i=1,2,3,4\right)$, where $R_{DS_i}=10\%, 40\%, 70\%, 100\%$ are defined to relate to $DS_i\left(i=1,2,3,4\right)$, respectively.

4.3 Seismic resilience assessment

Substituting Eq. (14) and Eq. (15) into Eq. (13), the values of R_{Loss} can be calculated by Eq. (12). Figure 11 shows the calculated R_{Loss} values of uncorroded and corroded frames, where the replacement treatment is adopted once the predefined replacement threshold is exceeded. In this study, the replacement threshold was determined once the repair cost exceeded 45% (Wen *et al.*, 2019). The replacement cost is defined by the initial cost times a factor of 1.25. Therefore, when the direct loss ratio reached beyond $1.25\times45\%=56\%$, the repair of a structure is not necessary; rather, a replacement is required.

As seen in Fig. 11, the calculated R_{Loss} values of the corroded frames are clearly greater than that of their uncorroded counterparts. Moreover, with growing corrosion levels, the corresponding R_{Loss} values are accordingly increased. The above observations show that reinforcement corrosion can lead to a promotion of the loss of resilience. To illustrate this promotion,

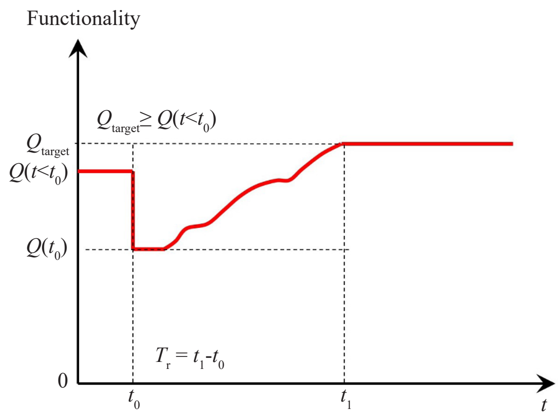

Fig. 10 Conceptual illustration for the loss factor of resilience

Table 7 Direct loss ratio considered in this study

$\theta_{\max}$	Damage state	Direct loss ratio
0–1%	DS_1	10%
1%–2%	DS_2	40%
2%–4%	DS_3	70%
>4%	DS_4	100%

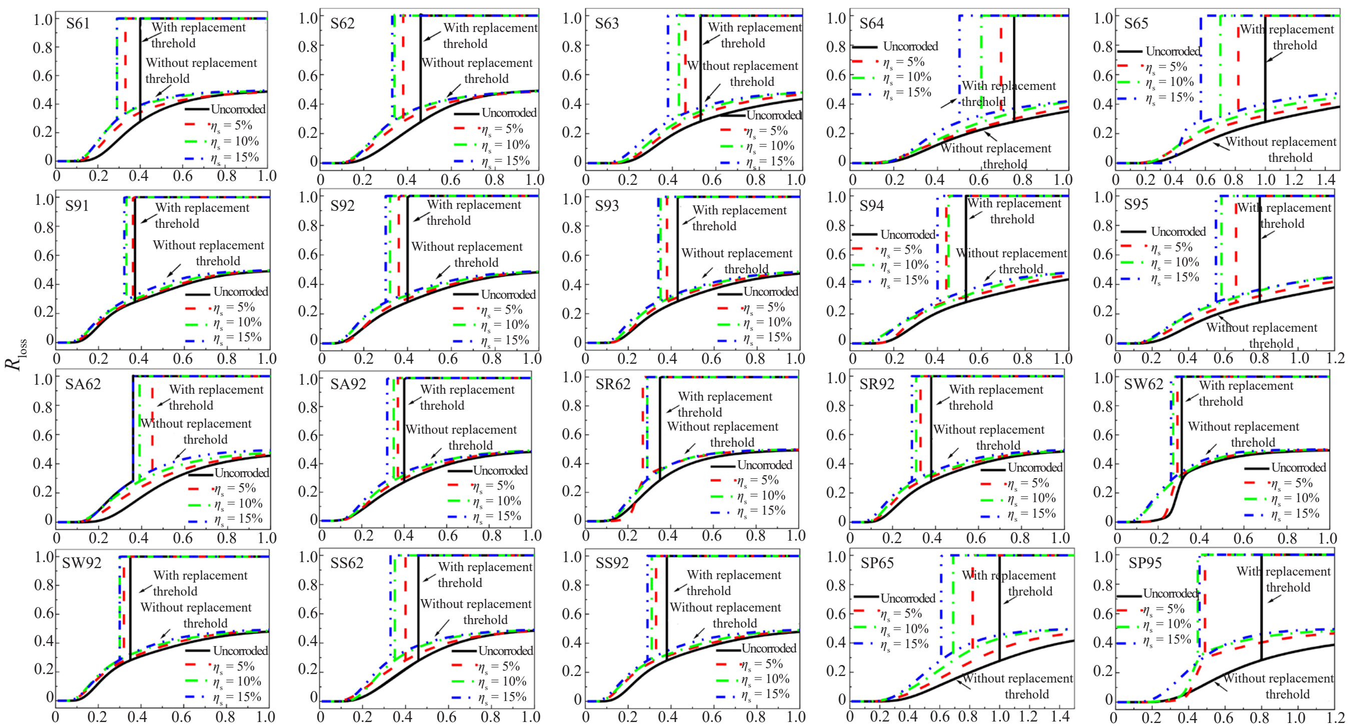

Fig. 11 Calculated loss factors of resilience for the case RC frames

Table 8 Seismic resilience loss ratios conditioned on the RE hazard level

Building	S_a values at RE	R_{loss} ($\times10^{-4}$) conditioned on RE			
		Uncorroded	η_s=5%	η_s=10%	η_s=15%
S61	0.1	1.48	18.26 (>200%)↑	51.57 (>200%)↑	52.33 (>200%)↑
S62	0.2	292.78	744.59 (154.3%)↑	1001.04 (>200%)↑	927.62 (>200%)↑
S63	0.3	913.06	1247.92 (36.7%)↑	1493.72 (63.6%)↑	1996.49 (118.6%)↑
S64	0.4	1919.8	1451.15 (-24.4%)↓	1584.82 (-17.4%)↓	2098.93 (9.32%)↑
S65	0.6	1435.86	2062.06 (43.6%)↑	2352.32 (63.8%)↑	2865.15 (99.5%)↑
S91	0.1	42.25	130.48 (>200%)↑	169.38 (>200%)↑	196.19 (>200%)↑
S92	0.2	1069.42	1112.28 (4.02%)↑	1701.95 (59.2%)↑	1760.55 (64.7%)↑
S93	0.3	1821.46	2124.23 (16.6%)↑	2368.35 (30%)↑	2523.54 (38.6%)↑
S94	0.4	2086.68	2617.3 (25.4%)↑	2514.24 (20.5%)↑	2819.59 (35.1%)↑
S95	0.6	2165.56	2545.85 (17.5%)↑	2888.26 (33.3%)↑	3004.06 (38.7%)↑
SA62	0.2	97.75	525.62 (>200%)↑	819.21 (>200%)↑	803.78 (>200%)↑
SA92	0.2	770.91	866.86 (12.5%)↑	1025.11 (32.9%)↑	1270.58 (64.9%)↑
SR62	0.2	811.01	275.79 (-66%)↓	1260.9 (55.5%)↑	1433.2 (76.7%)↑
SR92	0.2	860.87	1334.94 (55.1%)↑	1559.04 (81.1%)↑	1797.12 (108.7%)↑
SW62	0.6	156.14	130.37 (-16.7%)↓	1756.34 (>200%)↑	1960.16 (>200%)↑
SW92	0.2	1199.81	1573.02 (31.1%)↑	1762.11 (46.8%)↑	1684.11 (40.3%)↑
SS62	0.2	296.29	784.25 (164.9%)↑	615.62 (108.1%)↑	975.25 (>200%)↑
SS92	0.2	888.3	1557.05 (75.3%)↑	1666.24 (87.6%)↑	1818.72 (104.8%)↑
SP65	0.2	1098.3	1568.64 (42.9%)↑	2168.79 (97.5%)↑	2764.43 (151.7%)↑
SP95	0.6	1895.28	3436.62 (81.4%)↑	3849.64 (103.2%)↑	3893.06 (105.4%)↑

the R_{Loss} values conditioned on earthquake hazards at the rare earthquake (RE) were especially calculated for corroded and uncorroded RC frames, as shown in Table 8. It is noteworthy that the seismic performance of structures under three seismic hazards, i.e., frequent earthquake (FE), design basis earthquake (DBE), and RE, is concentrated in the Chinese seismic design code (GB50010-2010, 2010). At the FE and DBE hazard levels, the seismic damage to structures is commonly limited and therefore solely the RE hazard level was considered here for illustration. As seen from Table 8, reinforcement corrosion leads to significant growth of R_{Loss}. For the case frames, this growth can even exceed 200%, showing the huge effect of reinforcement corrosion on structural resilience.

5 Conclusions

This study conducted a comprehensive investigation on the seismic resilience of RC frame structures under corrosion. A total of twenty RC frames were designed according to Chinese seismic design codes for representing the typical construction in coastal China. In the structural designs, four important variables, the number of stories, bay width, axial loading ratio, and period reduction factor, were considered at low, medium, and high levels. A numerical finite element model was developed on the OpenSees platform to simulate the inelastic behaviors of corroded RC frames due to the effects of earthquakes, an approach verified by effectively simulating the cyclic loading test data of uncorroded and corroded RC columns. Reinforcement corrosion rates of 5%, 10%, and 15% were considered to represent low, medium, and high corrosion levels, respectively. The effect of reinforcement corrosion on structural performance was accounted for by degrading properties of reinforcement, concrete cover, and their bond-slip performance.

To quantify the seismic resilience of structures, a normalized loss factor of resilience was assessed for all the case frames by considering growing corrosion levels. As an important ingredient of resilience, the fragility relationships were first developed for the corroded and uncorroded case frames by considering three limit states: IO, CP, and LS. Compared to the uncorroded RC frame, the corroded frames showed larger failure probability at a specific limit state, illustrating the deterioration of the structural capacity due to the effects of earthquakes. Moreover, the effect of reinforcement corrosion on the corresponding fragility is limited at the IO limit state, whereas it is significant at the CP and LS limit states. It was found that the fragility medians of corroded RC frames were decreased with the corrosion rate of reinforcement. However, no clear trend was observed between fragility dispersions and corrosion rates.

The obtained loss of resilience for the corroded RC frames is significantly higher than that for their uncorroded counterparts. This reduction of resilience due to corrosion is aggregated with growing corrosion rates. At the Rare Earthquake hazard level, the corrosion-induced growth in the loss of resilience can even exceed 200%. This result reveals that reinforcement corrosion should not be neglected in the resilience assessment of structures. It is noteworthy that no clear trend was observed on the effect of the four important design variables that were considered—including the number of stories, bay width, axial loading ratio, and period reduction factor—on the fragility and resilience of corroded structures. This reflects the complexity of the effect of reinforcement corrosion on the seismic performance of RC structures. The above conclusions are limited to the cases in the current study. An additional study is being conducted to correlate structure-specific resilience with regional resilience, while incorporating the aging effect.

Acknowledgment

The research in this paper has received financial support from the National Natural Science Foundation of China (project number: 51778198), and the Natural Science Foundation for Excellent Young Scientists of Heilongjiang Province (project number: YQ2020E023).

References

Afsar DE, Rahmat M and Kashani MM (2018), "Probabilistic Seismic Vulnerability Analysis of Corroded Reinforced Concrete Frames Including Spatial Variability of Pitting Corrosion," *Soil Dynamics and Earthquake Engineering*, **114**: 97–112.

Ancheta TD, Darragh RB, Stewart JP, *et al*. (2013), "PEER NGA-West2 Database," *Pacific Earthquake Engineering Research Center*, PEER Report: 2013/03.

Bhargava K, Ghosh A, Mori Y, *et al.* (2007), "Corrosion-Induced Bond Strength Degradation in Reinforced Concrete-Analytical and Empirical Models," *Nuclear Engineering and Design*, **237**(11): 1140–1157.

Biondini F, Camnasio E, Titi A, *et al.* (2015), "Seismic Resilience of Concrete Structures Under Corrosion," *Earthquake Engineering & Structural Dynamics*, **44**(14): 2445–2466.

Bruneau M, Chang SE, Eguchi RT, *et al.* (2003), A Framework to Quantitatively Assess and Enhance the Seismic Resilience of Communities," *Earthquake Spectra*, **19**(4): 733–752.

Cairns J, Plizzari GA , Du Y, *et al*. (2005), "Mechanical Properties of Corrosion-Damaged Reinforcement," *ACI Materials Journal*, **102**(4): 256–264.

Chung L, Cho S, Kim JJ, *et al.* (2004), "Correction Factor Suggestion for ACI Development Length Provisions Based on Flexural Testing of RC Slabs with Various Levels of Corroded Reinforcing Bars," *Engineering Structures*, **26**(8): 1013–1026.

Cimellaro GP, Reinhorn AM, Bruneau M, *et al.* (2010), "Seismic Resilience of a Hospital System," *Structure and Infrastructure Engineering*, 127–144.

Cimellaro GP, Reinhorn AM, Bruneau M, *et al.* (2010), "Framework for Analytical Quantification of Disaster Resilience," *Engineering Structures*, **32**(11): 3639–3649.

Coronelli D and Gambarova P (2004), "Structural Assessment of Corroded Reinforced Concrete Beams: Modeling Guidelines," *Journal of Structural Engineering*, **130**(8): 1214–1224.

Dai KY, Yu XH, Lu DG (2020a), "Phenomenological Hysteretic Model for Corroded RC Columns," *Engineering Structures*, **210**: 110315.

Dai KY, Liu C, Lu DG and Yu XH (2020b), "Experimental Investigation on Seismic Behavior of Corroded RC Columns Under Artificial Climate Environment and Electrochemical Chloride Extraction: A Comparative Study," *Construction and Building Materials*, **242**: 118014.

D'Ayala D, Meslem AD, Vamvatsikos D, Porter K, Rossetto T, Crowley H and Silva V (2014), "GEM Guidelines for Analytical Vulnerability Assessment of Low/Mid-Rise Buildings-Methodology," *Vulnerability Global Component Project*.

Deierlein GG, Krawinkler H, Ma X, *et al.* (2011), "Earthquake Resilient Steel Braced Frames with Controlled Rocking and Energy Dissipating Fuses," *Steel Construction*, **4**(3): 171–175.

Du YG, Clark LA, Chan AHC, (2005), "Residual Capacity of Corroded Reinforcing Bars," *Magazine of Concrete Research*, **57**(3):135–147.

Ellingwood BR, Celik OC, Kinali K, *et al.* (2007), "Fragility Assessment of Building Structural Systems in Mid-America," *Earthquake Engineering & Structural Dynamics*, **36**(13): 1935–1952.

Enright MP and Frangopol DM (1998), "Probabilistic Analysis of Resistance Degradation of Reinforced Concrete Bridge Beams Under Corrosion," *Engineering Structures*, **20**(11): 960–971.

FEMA 273 (1997), *NEHRP Guidelines for the Seismic Rehabilitation of Buildings*, Federal Emergency Management Agency.

GB50010-2010 (2010), *Code for Design of Concrete Structures*, China Architecture and Building, Beijing.

GB50011-2010 (2010), *Code for Seismic Design of Buildings*, China Architecture and Building, Beijing.

Ghosh J and Padgett JE (2010), "Aging Considerations in the Development of Time-Dependent Seismic Fragility Curves," *Journal of Structural Engineering*, **136**(12): 1497–1511.

Howary HA and Mehanny SS (2011), “Seismic Vulnerability Evaluation of RC Moment Frame Buildings in Moderate Seismic Zones,” *Earthquake Engineering & Structural Dynamics*, **40**(2): 215–235.

Hueste MB and Bai J (2007), “Seismic Retrofit of a Reinforced Concrete Flat-Slab Structure: Part II — Seismic Fragility Analysis,” *Engineering Structures*, **29**(6): 1178–1188.

Kent DC and Park R (1971), “Flexural Members with Confined Concrete,” *Journal of the Structural Division*, **97**(7): 1969–1990.

Liu Q and Jiang H (2017), “Experimental Study on a New Type of Earthquake Resilient Shear Wall,” *Earthquake Engineering & Structural Dynamics*, **46**(14): 2479–2497.

Liu XJ, Jiang HJ and He LS (2017), “Experimental Investigation on Seismic Performance of Corroded Reinforced Concrete Moment-Resisting Frames,” *Engineering Structures*, **153**: 639–652.

Lu DG, Yu XH, Jia MM, *et al.* (2014), “Seismic Risk Assessment for a Reinforced Concrete Frame Designed According to Chinese Codes,” *Structure and Infrastructure Engineering*, **10**(10): 1295–1310.

Lundgren K (2007), “Effect of Corrosion on the Bond Between Steel and Concrete: An Overview,” *Magazine of Concrete Research*, **59**(6): 447–461.

Mander JB, Priestley MJN and Park R (1998), “Theoretical Stress-Strain Model for Confined Concrete,” *Journal of Structural Engineering*, **114**(8): 1804–1826.

Mckenna F (2011), “OpenSees: A Framework for Earthquake Engineering Simulation,” *Computing in Science and Engineering*, **13**(4): 58–66.

Miano A, Jalayer F, Ebrahimian H, *et al.* (2018), “Cloud to IDA: Efficient Fragility Assessment with Limited Scaling,” *Earthquake Engineering & Structural Dynamics*, **47**(5): 1124–1147.

Miles SB and Chang SE (2006), “Modeling Community Recovery from Earthquake,” *Earthquake Spectra*, **22**(2): 439–458.

Motlagh ZS, Dehkordi MR, Eghbali M, *et al.* (2020), “Evaluation of Seismic Resilience Index for Typical RC School Buildings Considering Carbonate Corrosion Effects,” *International Journal of Disaster Risk Reduction*, **46**: 101511.

Ning CL, Cheng Y and Yu XH (2019), “A Simplified Approach to Investigate the Seismic Ductility Demand of Shear-critical Reinforced Concrete Columns Based on Experimental Calibration,” *Journal of Earthquake Engineering*, DOI: 10.1080/13632469.2019.1605949

Ramamoorthy SK, Gardoni P, Bracci JM, *et al.* (2006) “Probabilistic Demand Models and Fragility Curves for Reinforced Concrete Frames,” *ASCE Journal of Structural Engineering*, **132**(10): 1563–1572.

Sabbagh AB, Petkovski M, Pilakoutas K, *et al.* (2012), “Experimental Work on Cold-Formed Steel Elements for Earthquake Resilient Moment Frame Buildings,” *Engineering Structures*, **42**: 371–386.

Scott MH and Fenves GL (2006), “Plastic Hinge Integration Methods for Force-Based Beam-Column Elements,” *ASCE Journal of Structural Engineering*, **132**(2): 244–252.

Shome N, Cornell CA, Bazzurro P, *et al.* (1998), “Earthquakes, Records, and Nonlinear Responses,” *Earthquake Spectra*, **14**(3): 469–500.

Wen WP, Zhang M, Zhai CH, *et al.* (2019), “Resilience Loss Factor for Evaluation and Design Considering the Effects of Aftershocks,” *Soil Dynamics and Earthquake Engineering*, 43–49.

Wen YK, Ellingwood BR and Bracci JM (2004), “Vulnerability Function Framework for Consequence-Based Engineering,” *Technical Report No. DS-4; US: Mid-America Earthquake Center* (*MAE*), University of Illinois at Urbana-Champaign.

Wilkinson S, Hurdman G, Crowther A, *et al.* (2006), “A Moment Resisting Connection for Earthquake Resistant Structures,” *Journal of Constructional Steel Research*, **62**(3): 295–302.

Xu SH (2003), “The Models of Deterioration and Durability Evaluation of Reinforced Concrete Structure,” *PhD Dissertation*, Xi'an University of Architecture and Technology. (in Chinese)

Yalciner H, Sensoy S and Eren O (2015), “Seismic Performance Assessment of a Corroded 50-Year-Old Reinforced Concrete Building,” *Journal of Structural Engineering*, **141**(12): 05015001.

Yu XH, Qian K, Lu DG and Li B (2017a), “Progressive Collapse Behavior of Aging Reinforced Concrete Structures Considering Corrosion Effects,” *ASCE Journal of Performance of Constructed Facilities*, **31**(4): 04017009.

Yu XH, Lu DG, Li B, *et al.* (2017b), “Relating Seismic Design Level and Seismic Performance: Fragility-Based Investigation of RC Moment-Resisting Frame Buildings in China,” *Journal of Performance of Constructed Facilities*, **31**(5): 04017075.

Yu XH, Li S, Lu DG and Tao J (2018), “Collapse Capacity of Inelastic Single-Degree-of-Freedom Systems Subjected to Mainshock-Aftershock Earthquake Sequences,” *Journal of Earthquake Engineering*, **24**(5): 803–826.

Zhao J and Sritharan S (2007), “Modeling of Strain Penetration Effects in Fiber-Based Analysis of Reinforced Concrete Structures,” *ACI Structural Journal*, **104**(2): 133–141.

Zhao YX, Dong JF, Ding HJ, *et al.* (2015), “Shape of Corrosion-Induced Cracks in Recycled Aggregate Concrete,” *Corrosion Science*, **98**: 310–317.